Imaging

DOI: 10.1002/anie.201308494

Copper-64-Alloyed Gold Nanoparticles for Cancer Imaging: Improved Radiolabel Stability and Diagnostic Accuracy**

*Yongfeng Zhao, Deborah Sultan, Lisa Detering, Sangho Cho, Guorong Sun, Richard Pierce, Karen L. Wooley, and Yongjian Liu**

Abstract: *Gold nanoparticles, especially positron-emitter-labeled gold nanostructures, have gained steadily increasing attention in biomedical applications. Of the radionuclides used for nanoparticle positron emission tomography imaging, radiometals such as ^{64}Cu have been widely employed. Currently, radiolabeling through macrocyclic chelators is the most commonly used strategy. However, the radiolabel stability may be a limiting factor for further translational research. We report the integration of ^{64}Cu into the structures of gold nanoparticles. With this approach, the specific radioactivity of the alloyed gold nanoparticles could be freely and precisely controlled by the addition of the precursor $^{64}CuCl_2$ to afford sensitive detection. The direct incorporation of ^{64}Cu into the lattice of the gold nanoparticle structure ensured the radiolabel stability for accurate localization in vivo. The superior pharmacokinetic and positron emission tomography imaging capabilities demonstrate high passive tumor targeting and contrast ratios in a mouse breast cancer model, as well as the great potential of this unique alloyed nanostructure for preclinical and translational imaging.*

Nanoparticles have been widely used in biomedical research, including drug delivery and molecular imaging.[1] Of the various diagnostic applications, radiolabeled nanoparticles for positron emission tomography (PET) and single photon emission computed tomography (SPECT) imaging have received special attention owing to their high sensitivity, unlimited tissue penetration, and translational capability.[2] The desirable nuclear properties and straightforward radiolabeling chemistry make ^{64}Cu ($t_{1/2} = 12.7$ h, β^+, 0.653 MeV [17%]) the most widely used positron emitter for nanoparticle molecular imaging.[3]

Generally, ^{64}Cu is conjugated to the surface or core of nanoparticles through macrocyclic chelators such as 1,4,7,10-tetraazacyclododecane-1,4,7,10-tetraacetic acid (DOTA, $\log k = 22.3$).[3b,4] However, the in vivo stability of chelated ^{64}Cu is not ideal, which often leads to the transchelation of ^{64}Cu to proteins, high uptake in nontargeted organs, and, therefore, the misinterpretation of PET images.[5] Other chelators, such as cross-bridged cyclams, afford improved kinetic stability compared to DOTA.[6] However, ligands of this type normally require harsh radiolabeling conditions, which are unfavorable for commonly used targeting moieties, such as peptides and antibodies.[7] Additionally, their conjugation onto nanoparticles is fairly complicated and there is no report to date of clinical materials that are produced by using this strategy. Owing to the rapidly increased applications of ^{64}Cu-labeled nanoparticles in preclinical PET imaging and translational research, there is a great need to develop a new approach to radiolabel nanoparticles with improved stability in order to eliminate the misinterpretation of PET images and non-necessary radiation burden.

Among various nanoparticles, gold nanoparticles (AuNPs) are of particular interest and have been used for many biomedical applications because of their versatile surface chemistry, biocompatibility, robust preparation, and stability.[1b,8] However, their ^{64}Cu radiolabeling has also been performed through chelators conjugated on the surface.[5b,9] It has been reported that at 24 h post intravenous injection, about 20% of ^{64}Cu dissociated from DOTA and was hypothesized to end up in the liver, thus raising significant concern about the diagnostic accuracy.[5,10] Currently, with the focus of translational research shifting from molecular imaging toward targeted delivery,[11] the misleading information caused by this conventional radiolabeling strategy might significantly limit the potential of AuNPs for PET imaging.

To address these concerns, many radiolabeling strategies have been developed, including the chelator-free strategy of using ^{64}Cu-porphysomes and direct incorporation of ^{198}Au into AuNPs, and have shown great potential for oncological applications.[12] Our approach explored a new strategy to radiolabel AuNPs for PET imaging, namely by alloying ^{64}Cu directly into the lattice of the nanostructure to prepare $^{64}CuAuNPs$.[12a,b] Although nonradioactive CuAuNPs have been largely used as catalysts for chemical reactions,[13] they have not been studied for biomedical applications. Compared to the conventional ^{64}Cu labeling strategy, alloyed $^{64}CuAuNPs$ provide significant advantages including: 1) greatly improved radiolabeling stability to ensure diagnostic accuracy; 2) straightforward surface modification to increase the con-

[*] Dr. Y. Zhao, D. Sultan, L. Detering, Prof. Y. Liu
Mallinckrodt Institute of Radiology
Washington University School of Medicine
St. Louis, MI 63110 (USA)
E-mail: liuyo@mir.wustl.edu
Prof. R. Pierce
Department of Medicine
Washington University School of Medicine (USA)
S. Cho, Dr. G. Sun, Prof. K. L. Wooley
Department of Chemistry, Texas A&M University (USA)

[**] This work was supported in part by a start-up fund from Mallinckrodt Institute of Radiology, Washington University, and by the Welch Foundation as the W. T. Doherty-Welch Chair in Chemistry (A-0001).

Supporting information for this article is available on the WWW under http://dx.doi.org/10.1002/anie.201308494.

trol of the AuNPs surface properties; 3) superior targeting efficiency without effects from macrocyclic chelators.

We began the synthesis with nonradioactive gold chloride ($HAuCl_4$) and copper(II) acetylacetonate ($[Cu(acac)_2]$) using oleylamine as a solvent and reductant. Typically, the reaction mixture was heated to 160 °C with a programmed increase of 3 °C min^{-1} and then held at this temperature for 2 h prior to cooling to room temperature. After centrifugation, the CuAuNPs were dispersed in hexanes to produce a homogeneous reddish solution. Furthermore, the CuAuNPs surface was modified with α-methyl ether- and ω-thiol-terminated poly(ethylene glycol) (mPEG-SH, MW = 5000 Da) to improve the in vivo blood circulation. Compared to pure AuNPs ($\lambda_{max} = 522$ nm) prepared under the same conditions, the UV/Vis absorption of CuAuNPs showed a 13 nm red-shift, which was consistent with previously reported data.[13b]

The integration of ^{64}Cu into AuNPs was performed by following the same procedure for preparing nonradioactive CuAuNPs, except for the extra addition of the $^{64}CuCl_2$ precursor prior to heating,[14] which presumably underwent ligand exchange with $[Cu(acac)_2]$. Transmission electron microscopy (TEM) imaging showed that as-prepared ^{64}CuAuNPs are round with a diameter of (9.4 ± 1.2) nm (Figure 1 a). The hydrodynamic size determined with dynamic light scattering showed a monodisperse distribution ((27 ± 3.2) nm; Figure S1 in the Supporting Information) with a zeta potential of (−1.8 ± 1.1) mV. Inductively coupled plasma mass spectrometry (ICP-MS) measurements after the decay of ^{64}Cu gave the elemental composition of these ^{64}CuAuNPs as $CuAu_9$. The UV absorption of ^{64}CuAuNPs was consistent with nonradioactive CuAuNPs (Figure 1 b), thus indicating the integration of ^{64}Cu into the structure of the nanoparticles. Moreover, the high-angle annular dark-field scanning TEM and energy dispersive X-ray spectroscopy (EDS) analyses showed a homogeneous distribution of Cu across the nanoparticle structures from the decayed ^{64}CuAuNPs, thus indicating ^{64}Cu was uniformly alloyed into the lattice of AuNPs (Figure S2). Owing to the trace amount of incorporation of ^{64}Cu, the UV peak of the nanoparticles did not change after the decay of ^{64}Cu to stable Ni and Zn, which actually warranted the optical properties of the ^{64}CuAuNPs for biomedical applications. The ICP-MS measurement of the decayed ^{64}CuAuNPs showed the concentration of Zn in sample was 0.33 μg L^{-1} and Ni was undetected, thus confirming the low concentration of ^{64}Cu in the alloyed nanoparticles. Importantly, by fixing the molar ratio of $HAuCl_4$ and $[Cu(acac)_2]$ and changing the initial activity of $^{64}CuCl_2$, the radioactivity of synthesized ^{64}CuAuNPs could be controlled to significantly improve the specific activity of ^{64}CuAuNPs, ensure the ultra-trace amount administration for in vivo studies, and afford the capability for highly-sensitive detection (Figure 1 c). When 104 MB of $^{64}CuCl_2$ was used, the specific activity of ^{64}CuAuNPs was 5.5 GBq nmol^{-1}. Considering the concentration of ^{64}Cu in the total amount of copper was less than 5 ‰,[15] this new radiolabeling strategy held great potential to increase the specific activity of ^{64}CuAuNPs for sensitive and specific detection. The integrity of ^{64}CuAuNPs was clearly demonstrated by using fast protein liquid chromatography (FPLC) analysis (Figure 1 d).

We next studied the radiolabeling stability of ^{64}CuAuNPs in three solutions including pH 7.4 phosphate buffered saline (PBS), pH 7.4 PBS with a challenging agent of ethylenediaminetetraacetic acid (EDTA, 2.5 mM),[14] and mouse serum, by incubating the nanoparticles at 37 °C for up to 48 h. As shown in Figure 2 and Figure S3 in the Supporting Information, the ^{64}CuAuNPs were stable in mouse serum without any degradation or translation up to 48 h, which was significantly better than the stability of ^{64}Cu-DOTA[5b] and ^{111}In-DOTA ($\log k = 23.9$)[2d,4b] in serum. Interestingly, owing to the slow oxidation process of Cu to CuO or Cu_2O on the ^{64}CuAuNP

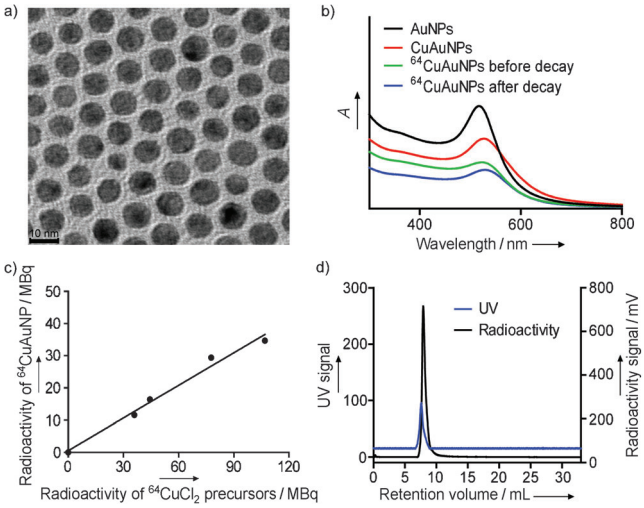

Figure 1. a) TEM image of the alloyed ^{64}CuAuNPs (diameter: (9.4 ± 1.2) nm) after decay. Scale bar: 10 nm. b) Normalized UV spectra of AuNPs, CuAuNPs, ^{64}CuAuNPs before decay, and ^{64}CuAuNPs after decay in aqueous solutions. c) Correlation of the radioactivities of the $^{64}CuCl_2$ precursor and synthesized ^{64}CuAuNPs ($R^2 = 0.98$). d) FPLC profile of ^{64}CuAuNPs on UV and radioactivity traces.

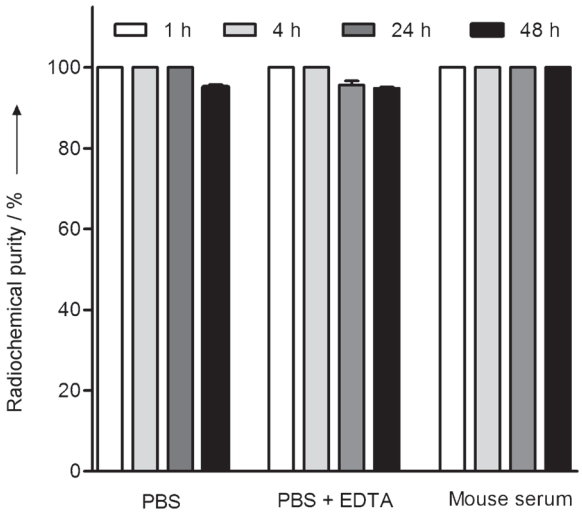

Figure 2. Radiolabel stability of alloyed ^{64}CuAuNPs in PBS buffer, PBS buffer with EDTA, and mouse serum, incubated at 37 °C at 1 h, 4 h, 24 h, and 48 h.

surface in aqueous solution,[13b] some ^{64}Cu may have been dissolved in PBS buffer and led to the value of (4.9 ± 0.6) % free ^{64}Cu after 48 h incubation. Furthermore, under the constant challenge of EDTA, the ^{64}CuAuNPs did not show any dissociation of ^{64}Cu from the nanoparticle, the (4.4 ± 1.0) % and (5.2 ± 0.3) % free ^{64}Cu at 24 h and 48 h post-incubation were largely due to the accelerated dissolution of ^{64}Cu in the presence of EDTA after the surface oxidation.[16]

In vivo pharmacokinetic evaluation of ^{64}CuAuNPs was performed in normal BALB/c mice to compare the distribution profiles (Figure 3). At 1 h postinjection (p.i.), most of the nanoparticles stayed in the systemic circulation with more than 60 %ID/g in blood pool organs (blood: (45.4 ± 2.49) %ID/g, lung (12.2 ± 1.19) %ID/g, heart: (6.42 ± 1.12) %ID/g) and low mononuclear phagocytic system (MPS) uptake including liver and spleen, which was consistent with previously reported results using similarly sized AuNPs.[17] Interestingly, the blood accumulation of this nanoparticle rapidly decreased at 24 h to a level of only 13.1 % of initial retention at 1 hour while the hepatic (2-fold) and splenic (5.5-fold) accumulations markedly increased. Owing to the small size of the ^{64}CuAuNPs, the sharp increase in the spleen accumulation actually indicated the in vivo stability of this nanoprobe because small particles would specifically accumulate in the spleen and the dissociated ^{64}Cu from the alloyed nanoparticle would mostly end up in the liver instead of the spleen.[10] However, further optimization needs to be performed to reduce the MPS system uptake for improved biodistribution profile. During the extended study to 48 h, the blood uptake of ^{64}CuAuNPs was further decreased to (1.28 ± 0.27) %ID/g, whereas the spleen and liver accumulations hardly changed. This type of distribution profile with high initial blood retention and fast clearance was consistent with previously reported gold nanostructures and favorable for the nanoparticles to achieve a high tumor-to-muscle (T/M) contrast ratio.[5b,12a]

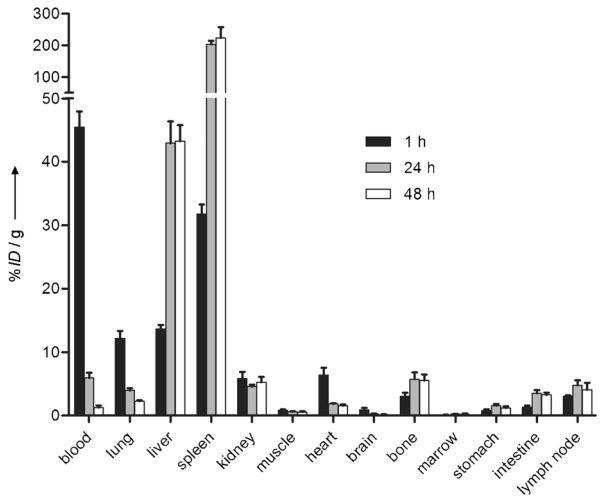

Figure 3. Biodistribution of alloyed ^{64}CuAuNPs in female BALB/c mice via tail vein administration at 1 h, 24 h, and 48 h post injection (n = 4/group)

We next studied the passive targeting capability of ^{64}CuAuNPs through the enhanced permeability and retention (EPR) effect in an EMT-6 mouse breast cancer model using a small animal PET/CT system. The tumor metabolism was also evaluated with the most commonly used tracer ^{18}F-fluorodeoxyglucose (^{18}F-FDG) in oncological imaging. This tumor model is known as a fast-growing model with active angiogenesis (Figure S4a). At 1 h p.i., consistent with the biodistribution profile, the PET/CT image of ^{64}CuAuNPs showed high blood pool retention, substantial MPS system accumulation, and low renal clearance in the EMT-6 tumor-bearing mouse (Figure 4a). The tumor uptake could be clearly visualized with an intensity ((4.93 ± 0.32) %ID/g) similar to that obtained with ^{18}F-FDG ((4.59 ± 0.43) %ID/g) at the same time point (Figure 4b). At 24 h p.i., with the clearance of ^{64}CuAuNPs from systemic circulation, the liver and spleen uptake levels became dominant. Since the EPR effect largely depends on leaky tumor vasculatures, the heterogeneous intra-tumoral distribution around the necrotic core was clearly profiled (Figure 4 and Figure S4b in the Supporting Information). Owing to the continuous accumulation of ^{64}CuAuNPs in the tumor, the quantitative tumor

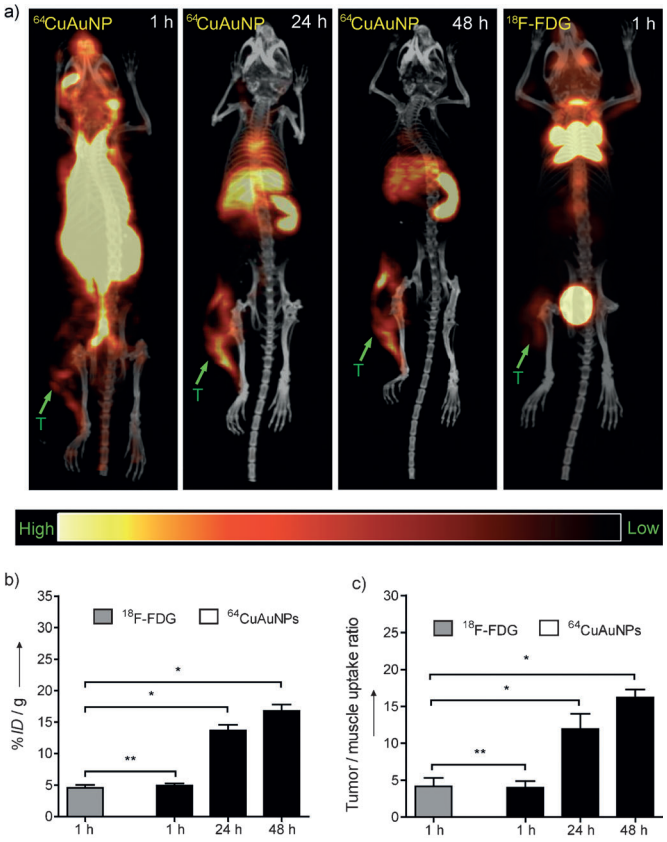

Figure 4. a) Representative PET/CT images at 1 h, 24 h, 48 h post-injection of alloyed ^{64}CuAuNPs and ^{18}F-FDG at 1 h in EMT-6 tumor-bearing mice (green arrow T: tumor). b) Quantitative tumor uptakes of alloyed ^{64}CuAuNPs and ^{18}F-FDG at various time points (*: $p < 0.05$; **: $p > 0.05$, $n = 4$). c) Tumor/muscle ratios of alloyed ^{64}CuAuNPs and ^{18}F-FDG at studied time points (*: $p < 0.05$; **: $p > 0.05$, $n = 4$).

uptake was increased almost twofold and the T/M ratio was significantly improved from 3.99 ± 0.89 to 11.9 ± 2.08 ($p < 0.05$, $n = 4$; Figure 4c). Importantly, when the PET/CT imaging was extended to 48 h -p.i., owing to the persistent retention of ^{64}CuAuNPs, the tumor uptake was further increased to (16.8 ± 0.98) %ID/g and the T/M ratio was also enhanced to 16.2 ± 1.07, which demonstrated the advantage of extended pharmacokinetics of nanoparticle for tumor PET imaging. Consistent with the PET/CT imaging, the dynamic autoradiography imaging also demonstrated the heterogeneous distribution of ^{64}CuAuNPs across the tumor mass (Figure S5 in the Supporting Information).

In summary, we have demonstrated a new ^{64}Cu radiolabeling strategy for gold nanoparticles and assessed their in vivo pharmacokinetics and PET imaging capability in a mouse breast cancer model. The direct incorporation of ^{64}Cu into the lattices of AuNPs afforded stable radiolabeling and precise control of the specific activity of these ^{64}CuAuNPs by varying the initial activity of the $^{64}CuCl_2$ precursor. This new radiolabeling strategy allows the development of high specific activity, stably labeled ^{64}CuAuNPs for accurate tracking of their in vivo fate and minimizes the misinterpretation of PET imaging results. The high initial blood retention and fast MPS system clearance of ^{64}CuAuNPs in mice led to accumulative tumor uptake and increased T/M ratio with the extension of PET imaging. Both PET and autoradiography confirmed the heterogeneous distribution profile across the tumor. This study demonstrated the potential of ^{64}CuAuNPs as a platform for further oncological PET imaging and may serve as a point of entry for a broader range of biomedical applications of positron-emitter-alloyed nanoparticles in preclinical and translational research. Current efforts are directed towards developing a more straightforward strategy to prepare the ^{64}Cu-alloyed AuNPs, reducing the size of the ^{64}CuAuNPs to reduce the MPS system accumulation, and increase the renal clearance for better contrast effect.

Received: September 30, 2013
Published online: November 24, 2013

Keywords: copper · gold · nanostructures · positron emission tomography · radiochemistry

[1] a) M. Elsabahy, K. L. Wooley, *Chem. Soc. Rev.* **2012**, *41*, 2545 – 2561; b) C. M. Cobley, J. Chen, E. C. Cho, L. V. Wang, Y. Xia, *Chem. Soc. Rev.* **2011**, *40*, 44 – 56; c) O. C. Farokhzad, R. Langer, *ACS Nano* **2009**, *3*, 16 – 20; d) H. Hong, Y. Zhang, J. Sun, W. Cai, *Nano Today* **2009**, *4*, 399 – 413.

[2] a) A. Louie, *Chem. Rev.* **2010**, *110*, 3146 – 3195; b) M. J. Welch, C. J. Hawker, K. L. Wooley, *J. Nucl. Med.* **2009**, *50*, 1743 – 1746; c) Z. Cheng, A. Al Zaki, J. Z. Hui, V. R. Muzykantov, A. Tsourkas, *Science* **2012**, *338*, 903 – 910; d) R. Rossin, P. R. Verkerk, S. M. van den Bosch, R. C. Vulders, I. Verel, J. Lub, M. S. Robillard, *Angew. Chem.* **2010**, *122*, 3447 – 3450; *Angew. Chem. Int. Ed.* **2010**, *49*, 3375 – 3378.

[3] a) Y. Guo, T. Aweda, K. C. Black, Y. Liu, *Curr. Top. Med. Chem.* **2013**, *13*, 470 – 478; b) Y. Liu, M. J. Welch, *Bioconjugate Chem.* **2012**, *23*, 671 – 682.

[4] a) G. Anderegg, F. Arnaud-neu, R. Delgado, J. Felcman, P. Konstantin, *Pure Appl. Chem.* **2005**, *77*, 1445 – 1495; b) T. J. Wadas, E. H. Wong, G. R. Weisman, C. J. Anderson, *Chem. Rev.* **2010**, *110*, 2858 – 2902.

[5] a) C. A. Boswell, X. Sun, W. Niu, G. R. Weisman, E. H. Wong, A. L. Rheingold, C. J. Anderson, *J. Med. Chem.* **2004**, *47*, 1465 – 1474; b) Y. Wang, Y. Liu, H. Luehmann, X. Xia, P. Brown, C. Jarreau, M. Welch, Y. Xia, *ACS Nano* **2012**, *6*, 5880 – 5888.

[6] L. Wei, Y. Ye, T. J. Wadas, J. S. Lewis, M. J. Welch, S. Achilefu, C. J. Anderson, *Nucl. Med. Biol.* **2009**, *36*, 277 – 285.

[7] R. A. De Silva, S. Jain, K. A. Lears, H. S. Chong, C. S. Kang, X. Sun, B. E. Rogers, *Nucl. Med. Biol.* **2012**, *39*, 1099 – 1104.

[8] a) R. A. Sperling, P. Rivera Gil, F. Zhang, M. Zanella, W. J. Parak, *Chem. Soc. Rev.* **2008**, *37*, 1896 – 1908; b) D. A. Giljohann, D. S. Seferos, W. L. Daniel, M. D. Massich, P. C. Patel, C. A. Mirkin, *Angew. Chem.* **2010**, *122*, 3352 – 3366; *Angew. Chem. Int. Ed.* **2010**, *49*, 3280 – 3294.

[9] M. Tian, W. Lu, R. Zhang, C. Xiong, J. Ensor, J. Nazario, J. Jackson, C. Shaw, K. A. Dixon, J. Miller, K. Wright, C. Li, S. Gupta, *Mol. Imaging Biol.* **2013**, *15*, 614 – 624.

[10] J. T. Jørgensen, M. Persson, J. Madsen, A. Kjær, *Nucl. Med. Biol.* **2013**, *40*, 345 – 350.

[11] a) S. M. Moghimi, D. Peer, R. Langer, *ACS Nano* **2011**, *5*, 8454 – 8458; b) J. R. McCarthy, J. Bhaumik, M. R. Karver, S. Sibel Erdem, R. Weissleder, *Mol. Oncol.* **2010**, *4*, 511 – 528.

[12] a) Y. Wang, Y. Liu, H. Luehmann, X. Xia, D. Wan, C. Cutler, Y. Xia, *Nano Lett.* **2013**, *13*, 581 – 585; b) R. Shukla, N. Chanda, A. Zambre, A. Upendran, K. Katti, R. R. Kulkarni, S. K. Nune, S. W. Casteel, C. J. Smith, J. Vimal, E. Boote, J. D. Robertson, P. Kan, H. Engelbrecht, L. D. Watkinson, T. L. Carmack, J. R. Lever, C. S. Cutler, C. Caldwell, R. Kannan, K. V. Katti, *Proc. Natl. Acad. Sci. USA* **2012**, *109*, 12426 – 12431; c) T. W. Liu, T. D. MacDonald, J. Shi, B. C. Wilson, G. Zheng, *Angew. Chem.* **2012**, *124*, 13305 – 13308; *Angew. Chem. Int. Ed.* **2012**, *51*, 13128 – 13131; d) T. W. Liu, T. D. MacDonald, C. S. Jin, J. M. Gold, R. G. Bristow, B. C. Wilson, G. Zheng, *ACS Nano* **2013**, *7*, 4221 – 4232.

[13] a) Y. Liu, A. R. Walker, *Angew. Chem.* **2010**, *122*, 6933 – 6937; *Angew. Chem. Int. Ed.* **2010**, *49*, 6781 – 6785; b) Z. Xu, E. Lai, Y. Shao-Horn, K. Hamad-Schifferli, *Chem. Commun.* **2012**, *48*, 5626 – 5628.

[14] Y. Liu, E. D. Pressly, D. R. Abendschein, C. J. Hawker, G. E. Woodard, P. K. Woodard, M. J. Welch, *J. Nucl. Med.* **2011**, *52*, 1956 – 1963.

[15] D. Zeng, C. J. Anderson, *Chem. Commun.* **2013**, *49*, 2697 – 2699.

[16] H. Tamura, N. Ito, M. Kitano, S. Takasaki, *Corros. Sci.* **2001**, *43*, 1675 – 1691.

[17] G. Zhang, Z. Yang, W. Lu, R. Zhang, Q. Huang, M. Tian, L. Li, D. Liang, C. Li, *Biomaterials* **2009**, *30*, 1928 – 1936.

